Interannual Variability of the Coupled Tropical Pacific Ocean–Atmosphere System Associated with the El Niño–Southern Oscillation

RONG-HUA ZHANG AND SYDNEY LEVITUS

Ocean Climate Laboratory, National Oceanographic Data Center/NOAA, Silver Spring, Maryland

(Manuscript received 15 November 1995, in final form 4 November 1996)

ABSTRACT

Upper-ocean temperature and surface marine meteorological observations are used to examine interannual variability of the coupled tropical Pacific climate system. The basinwide structure and evolution of meteorological and oceanographic fields associated with ENSO events are described using composites, empirical orthogonal functions, and a lagged correlation analysis.

The analyses reveal well-defined spatial structures and coherent phase relations among various anomaly fields. There are prominent seesaw patterns and orderly movement of subsurface ocean thermal anomalies. During an El Niño year, positive temperature anomalies occur in the eastern and central tropical Pacific upper ocean. Westerly wind anomalies, displaced well to the west of SST anomalies, occur over the western and central equatorial region. These patterns are accompanied by subsurface negative temperature anomalies in the west, with maxima located at thermocline depths off the equator. A reverse pattern is observed during La Niña.

The ENSO evolution is characterized by a very slow propagation of subsurface thermal anomalies around the tropical Pacific basin, showing consistent and coherent oceanic variations in the west and in the east, at subsurface depths and at the sea surface, and on the equator and off the equator of the tropical North Pacific. A common feature associated with the onset of El Niño is an appearance of subsurface thermal anomalies in the western Pacific Ocean, which propagate systematically eastward along the equator. Their arrival to the east results in a reversal of SST anomaly polarity, which then correspondingly produces surface wind anomalies in the west, which in turn produce and intensify the subsurface anomalies off the equator, thus terminating one phase of the Southern Oscillation. At the same time, the continual anomaly movement at depth from east to west off the equator provides a phase transition mechanism back to the west. In due course, opposite anomalies are located in the subsurface equatorial western Pacific, introducing an opposite SO phase and beginning a new cycle. Therefore, the phase transitions at the sea surface in the east and at depth in the west are both caused by these preferential, slowly propagating subsurface temperature anomalies, which are essential to the ENSO evolution. Their cycling time around the tropical Pacific basin may determine the period of the El Niño occurrence.

The authors' data analyses show an important role of the thermocline displacement in producing and phasing SST anomalies in the eastern and central equatorial Pacific. The coherent subsurface anomaly movement and its phase relation with SST and surface winds determine the nature of interannual variability and provide an oscillation mechanism for the tropical Pacific climate system. It appears that interannual variability represents a slowly evolving air–sea coupled mode, rather than individual free oceanic Rossby and Kelvin wave modes. These results provide an observational basis for verifying theoretical studies and model simulations.

1. Introduction

The El Niño–Southern Oscillation (ENSO) is the most prominent phenomenon of interannual variability in the tropical Pacific Ocean–atmosphere system. Bjerknes (1969) first proposed that unstable interactions between the ocean and atmosphere are responsible for ENSO episodes. Since then, extensive research has been conducted to describe its spatial structure and time evolution and to understand physical processes and mechanisms operating in the coupled system.

Theoretical studies have suggested many possible mechanisms and processes that elucidate important dynamical regimes in coupled tropical air–sea interactions, helping to explain the remarkable differences and diversity of the ENSO behavior and evolution (e.g., Hirst 1986; Jin and Neelin 1993). Numerical simulations have been one of the most powerful tools for describing and understanding interannual variability associated with ENSO, and for providing comprehensive views of the complicated, nonlinear climate system. In particular, ENSO-like events have been simulated by numerical models of varying complexity (Cane and Zebiak 1985; Zebiak and Cane 1987; Schopf and Suarez 1988; Battisti and Hirst 1989; Neelin 1990; Lau et al. 1992; Philander et al. 1992; Nagai et al. 1992; Latif et al. 1993; Zhang et al. 1995). These studies have greatly improved our understanding of the ENSO phenomenon. At the same

Corresponding author address: Dr. Rong-Hua Zhang, Graduate School of Oceanography, University of Rhode Island, Narragansett, RI 02882.
E-mail: zrh@sequan.gso.uri.edu

time, they also show a great sensitivity of model results to physical parameters and to model formulation. Furthermore, there are considerable discrepancies in comparison with the corresponding observations, and there are substantial intermodel differences (Philander et al. 1989; Neelin et al. 1992). In fact, results from theoretical studies and numerical simulations require verification against the corresponding basinwide observations, particularly of subsurface ocean thermal variability (Philander et al. 1992; Chao and Philander 1993).

Observational analyses for meteorological aspects of ENSO events have been conducted intensively and extensively. Various studies involve different methods of analyses and focus on different aspects of the phenomena (e.g., Rasmusson and Wallace 1983; Wright and Wallace 1988). In particular, the tropical Pacific atmospheric evolution in response to the changing sea surface temperatures (SSTs) has been described in detail by Rasmusson and Carpenter (1982). Oceanographic studies of the ENSO phenomenon are also numerous. Observations obtained at the sea surface (sea level and SST) have been of particular importance and have been analyzed in detail (e.g., Wyrtki 1975, 1985; Fu et al. 1986). The dominant mode of interannual variability is identified as an ENSO-related signal. Recently, subsurface ocean data and their derived variables such as dynamic height, heat content, and the 20°C isotherm depth have been analyzed (White et al. 1985, 1989; Kessler 1990; McPhaden et al. 1990; Levitus et al. 1994b; Tourre and White 1995; Kessler and McPhaden 1995; Zhang and Levitus 1996). These individual analyses for various atmospheric and oceanic components have shown that there are intrinsically well-defined spatial patterns among different climate parameters with coherent time evolution. As observed, and as demonstrated by theoretical studies and numerical simulations, the ocean and atmosphere are strongly coupled. Not only are anomaly fields highly correlated in space and time, but different atmospheric and oceanic variables are correlated with one another. Some combined interannual variability of the coupled atmosphere–ocean system has recently been analyzed but with heavily weighted emphasis on the atmospheric component because of the lack of subsurface ocean data (Wang 1992; Nigam and Shen 1993). Furthermore, it is becoming increasingly evident that the subsurface ocean may provide a memory mechanism responsible for the low-frequency oscillation in the coupled climate system. In particular, two theories have been put forward to explain the ENSO dynamics and its interannual cycle. One suggests (based on sea level observations and model simulations) that the buildup and release of ocean heat content in the equatorial and off-equatorial regions is important in setting up the spatial and temporal scale for ENSO (Wyrtki 1975, 1985; Cane et al. 1986; Zebiak 1989; Springer et al. 1990). Another is the delayed oscillator mechanism, with emphasis on individual equatorial wave dynamics in the ocean (Schopf and Suarez 1988; Battisti and Hirst 1989). Some limited observations have been given; some support it but others do not (Li and Clarke 1994; Mantua and Battisti 1994; Kessler and McPhaden 1995; Picaut and Delcroix 1995; Boulanger and Menkes 1995; Zhang and Levitus 1996). In addition, the role of ocean equatorial and off-equatorial Rossby waves in the ENSO cycle has been a subject of recent debate (Battisti 1989; Graham and White 1988, 1991; Kessler 1991). It is, therefore, important to analyze basinwide subsurface records, together with surface marine data, to describe the ENSO cycle in the real world as well as to evaluate theories and model simulations.

Recently, Levitus et al. (1994b) produced yearly temperature anomaly fields for the upper global ocean. Analyses of these fields suggest they are valuable for describing and understanding interannual variability of the ocean circulation, as well as for verifying results from theoretical studies and numerical simulations, and guiding field experiments (Levitus et al. 1994a,b; Zhang and Levitus 1996). Thus, these oceanic datasets, together with analyses based on the Comprehensive Ocean–Atmosphere Data Set (COADS) (Woodruff et al. 1987; Da Silva et al. 1994a,b) offer a possibility of systematically describing the basinwide structure and time evolution of the coupled interannual variability associated with ENSO cycle in a consistent way.

A brief description of the data sources and processing procedures is given in section 2. Some characteristic structure and evolution of interannual variations in the tropical Pacific are described briefly in section 3. The composite structure during El Niño and La Niña years is given in section 4. Using results of EOF analyses, the principal modes of ENSO are examined in section 5. The space–time evolution associated with ENSO cycle is examined in section 6 based on a lagged correlation analysis. Section 7 briefly evaluates current ENSO theories and model simulations based on our data analyses. Finally, section 8 gives summary.

2. Observational data

The data include yearly atmospheric and oceanic anomalies in the tropical Pacific: sea surface zonal and meridional wind components; sea level pressure (SLP); the 20°C isotherm depth; temperature at the upper ocean standard levels of sea surface; 10-, 20-, 30-, 50-, 75-, 100-, 125-, 150-, 200-, 250-, 300-, and 400-m depths; and heat content (HC, vertically averaged temperature anomalies in the upper 300 m of the water column).

The atmospheric variables were based on the analyses of surface marine anomalies (Da Silva et al. 1994a,b), which were derived from individual COADS observations from January 1945 to December 1989 (Woodruff et al. 1987). The raw observations were objectively analyzed with the same analysis scheme used by Levitus and Boyer (1994) and on the same 1° global grid to produce monthly mean anomaly fields.

The oceanic data used in the paper were the yearly

in situ temperature anomaly fields given by Levitus et al. (1994b). These fields represent objective analyses of all historical temperature profiles available at the National Oceanographic Data Center through November 1993, including data made available from the IOC Global Oceanographic Data Archaeology and Rescue Projects (Levitus et al. 1994c). These observational profiles have been analyzed in a consistent, objective manner on a 1° latitude–longitude grid at standard oceanographic analysis levels between the sea surface and a depth of 400 m. Briefly, the observed temperature profiles were first subjected to quality control checks to identify any unrealistic data. After this, the observed level data were vertically interpolated to the standard levels. To remove the annual cycle, the standard level values of each temperature profile were subtracted from the corresponding climatological monthly mean temperature values to produce a set of anomaly profiles. Then, the anomaly profiles were composited by 1-yr periods on a 1° grid at each upper-ocean standard level. Finally, these 1° square anomaly fields were objectively analyzed to produce values on a 1° latitude–longitude grid. Data sources, quality control, and analysis procedure are described in detail by Levitus et al. (1994b,c), together with distribution of temperature observations at the selected upper-ocean standard levels during the annual compositing period for each year from 1960 to 1990.

For the present work, the 1° atmospheric and oceanic anomaly fields were averaged to produce datasets on a 5° latitude–longitude grid. The yearly atmospheric anomalies are departures from the 1961–89 mean values and the yearly oceanic anomalies are those from the 1961–90 mean values. For our EOF analyses, the observed data at a given grid point have been normalized by the standard deviation so that the elements of the matrix are actually correlation coefficients.

3. Interannual variations

The basic observations are presented in this section in order to demonstrate a brief overview of interannual variations, phase propagation behavior, and interrelationships among various atmospheric and oceanic anomalies associated with ENSO evolution, before showing more elaborate analyses in the following sections.

Figure 1 shows interannual SLP variations along the equator and along 15°N, respectively. The SO can be clearly seen as a seesaw structure of anomaly pattern in the west and in the east over the tropical Pacific. During the warm phase of SO—that is, El Niño—SLP anomalies are positive in the west but negative in the east. The opposite patterns are observed during the La Niña phase. Another feature is an eastward propagation of SLP anomalies both along the equator and off the equator of the tropical Pacific. These anomalies seem to originate from the western Pacific and take 1–2 yr to move across the basin.

Figure 2 shows the interannual variations in surface zonal winds and SST along the equator. The largest interannual fluctuations in the zonal winds are found in the western and central equatorial Pacific, but those in SST are located in the central and eastern equatorial regions. The warm and cold events can be clearly seen—that is, El Niño conditions in years 1972, 1976, 1979, 1982, and 1986 and La Niña conditions in years 1971, 1973, 1975, 1984, and 1988. Some propagation features can be seen but are largely confined to the eastern Pacific in SST and to the western Pacific in zonal winds.

Examination of temperature anomaly distributions from the sea surface to subsurface depths shows considerable changes in the magnitude of the variability, structure, and propagation characteristics (Levitus et al. 1994b; Zhang and Levitus 1996). Figure 3 shows the interannual variations in heat content along the equator and along 15°N. There is large variability in the western as well as eastern Pacific Ocean. A very slow propagation of the ocean heat content anomalies is strikingly apparent around the tropical Pacific basin. In particular, there is a systematic and coherent eastward phase propagation along the equator associated with El Niño and La Niña events. The time required for an anomaly to cross the equatorial Pacific is about 1–2 yr.

Recently, Kessler and McPhaden (1995), analyzing the high temporal resolution temperature observations made by the Tropical Atmosphere–Ocean buoy array, also note a slow eastward propagation of the 20°C isotherm depth anomalies during the 1991–93 El Niño. They further demonstrate that the detection of propagation signals strongly depends on data sampling. On the interannual timescale with a 13-month running mean performed on the observations, Kelvin wave and equatorial Rossby wave signals cannot be revealed explicitly. Instead, the slow eastward propagating signal stands out along the equator.

Large interannual variations also appear in the off-equatorial region (Fig. 3b). Unlike the variations along the equator, those along 15°N are characterized by westward phase propagation. In addition, there is a hint of anomaly phase continuity of equatorial and off-equatorial signals in the tropical Pacific Ocean. This is more evident in the horizontal distributions of anomalies for subsurface temperature, 20°C isotherm depth, and heat content. An example of the basinwide heat content evolution is shown in Fig. 4 for years 1982 through 1987. Heat content anomalies can be seen to develop in the tropical western Pacific and move into the equatorial waveguide, and then propagate systematically eastward along the equator. There is a clear indication of westward moving anomalies off the equator of the tropical North Pacific as well. Based on Figs. 3–4, and the geographic distribution of temperature anomaly fields given by Levitus et al. (1994b), the heat content evolution during 1982–87 can be briefly described as follows. In 1982, an El Niño condition prevails in the tropical Pacific Ocean: there is a significant negative anomaly in the western Pacific and a positive anomaly in the east.

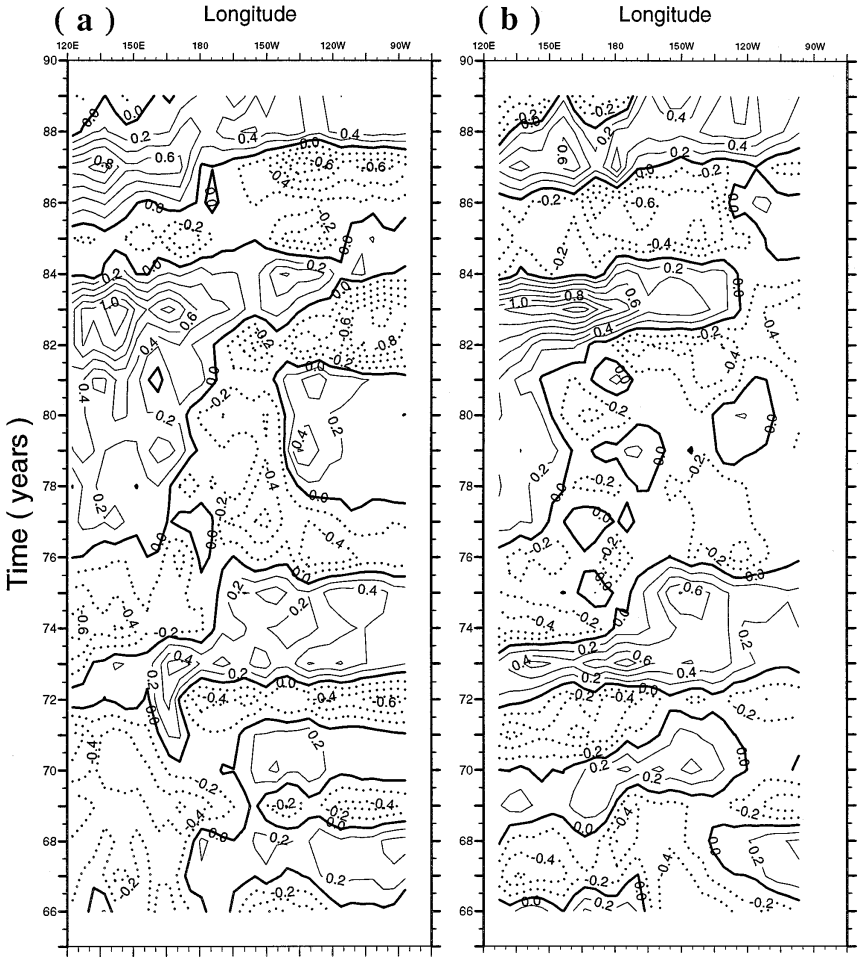

FIG. 1. Interannual variations in sea level pressure (mb) (a) along the equator and (b) along 15°N from 1966 to 1990. The contour interval is 0.2 mb, with dotted line indicating negative anomalies.

These anomalies propagate eastward along the equator. In 1983, the negative anomalies cover a large portion of the equatorial Pacific while the positive anomalies have moved northward along the North American coast and move toward the mid–Pacific Ocean in the off-equatorial tropical North Pacific (Figs. 4b,c). Then, these anomalies appear to continue their phase propagation: eastward along the equator but westward off the equator. In particular, the positive anomalies have moved westward across the whole tropical North Pacific and arrive at the western boundary regions in 1984 (Fig. 4c). Subsequently, the positive anomalies, after their extension into the equatorial waveguide, seem to move eastward along the equator and arrive at the eastern and coastal equatorial Pacific in 1986 (an El Niño year). At the same time, a significant negative anomaly is found in the west (Fig. 4e). The spatial pattern in 1986 is similar to that in 1982, thus indicating a completion of one cycle. Then, these anomalies continue to propagate eastward along the equator and westward off the equator. One year later (in 1987), the negative anomalies have propagated across the equatorial Pacific. Consequently, warm conditions in the east decay, and are replaced by negative polarity, and another La Niña occurs in 1988. Meanwhile, the positive anomalies centered in the eastern Pacific in 1986 (Fig. 4e) have propagated off the equator across the tropical North Pacific. Note that the spatial structures of anomaly patterns in 1984 and in 1987 are similar.

The space–time evolution of the heat content anomalies suggests preferential phase propagation consisting of an interannual cycle in the regions of the equatorial waveguide, off-equatorial tropical North Pacific, and eastern and western boundaries. The coherent patterns in the ocean and atmosphere indicate that interannual variability represents a slowly evolving air–sea coupled mode.

4. Composite structure during El Niño and La Niña years

Composite structure and evolution of the atmospheric anomalies in response to the SST variations have been described in many studies (e.g., Rasmusson and Car-

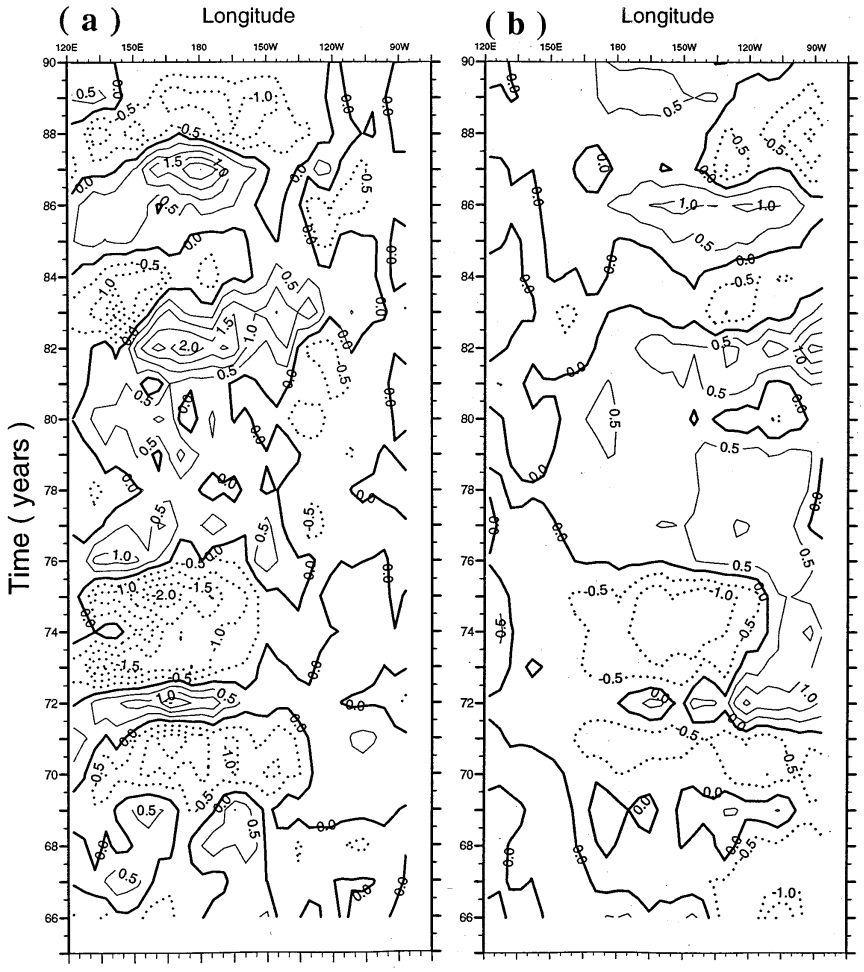

FIG. 2. Interannual variations in (a) surface zonal winds and (b) SST along the equator from 1966 to 1990. The contour intervals are 0.5 m s^{-1} and 0.5°C, respectively, with dotted line indicating negative anomalies.

penter 1982; Wright and Wallace 1988). However, the basinwide structure including subsurface oceanic thermal anomalies has not been described in detail from observational data. Note that Chao and Philander (1993) gave results based on an ocean general circulation model forced by the observed winds, and summarized the spatial patterns of surface winds, SST, and heat storage at the peak phases of El Niño and La Niña. To provide an observational basis, we present in this section the composite structure of the atmospheric and oceanic anomalies during El Niño and La Niña years.

During the period 1961–89, several El Niño and La Niña events occurred. We composite annual anomaly fields for five warm episodes (years 1972, 1976, 1979, 1982, and 1986) and five cold episodes (years 1971, 1973, 1975, 1984, and 1988) to simply describe the spatial structure of El Niño and La Niña, respectively.

Figure 5 shows the composite anomalies of sea surface winds (vectors), 20°C isotherm depth, SST, and temperature at 125-m depth for El Niño. Positive SST anomalies are located in the central and eastern tropical Pacific Ocean, but those in the western Pacific are negative and small. This is accompanied by eastward surface wind anomalies in the western and central equatorial Pacific, displaced well to the west of the SST anomalies. In the eastern equatorial Pacific, the wind anomalies are out of phase with those in the west, with easterly wind anomalies over the positive SST anomalies. In the western North (South) Pacific, there are notable anticyclonic (cyclonic) circulation anomalies that coincide coherently with a thermal anomaly pattern at subsurface depths. In addition, there are anomalous northerly winds in the tropical northeastern Pacific, suggesting a southward displacement of the intertropical convergence zone (ITCZ). Also, there is an indication of a northward movement of the South Pacific convergence zone (SPCZ) in the western South Pacific, manifested as southerly wind anomalies.

Although the major sea surface warming area during an El Niño is confined to the central and eastern tropical

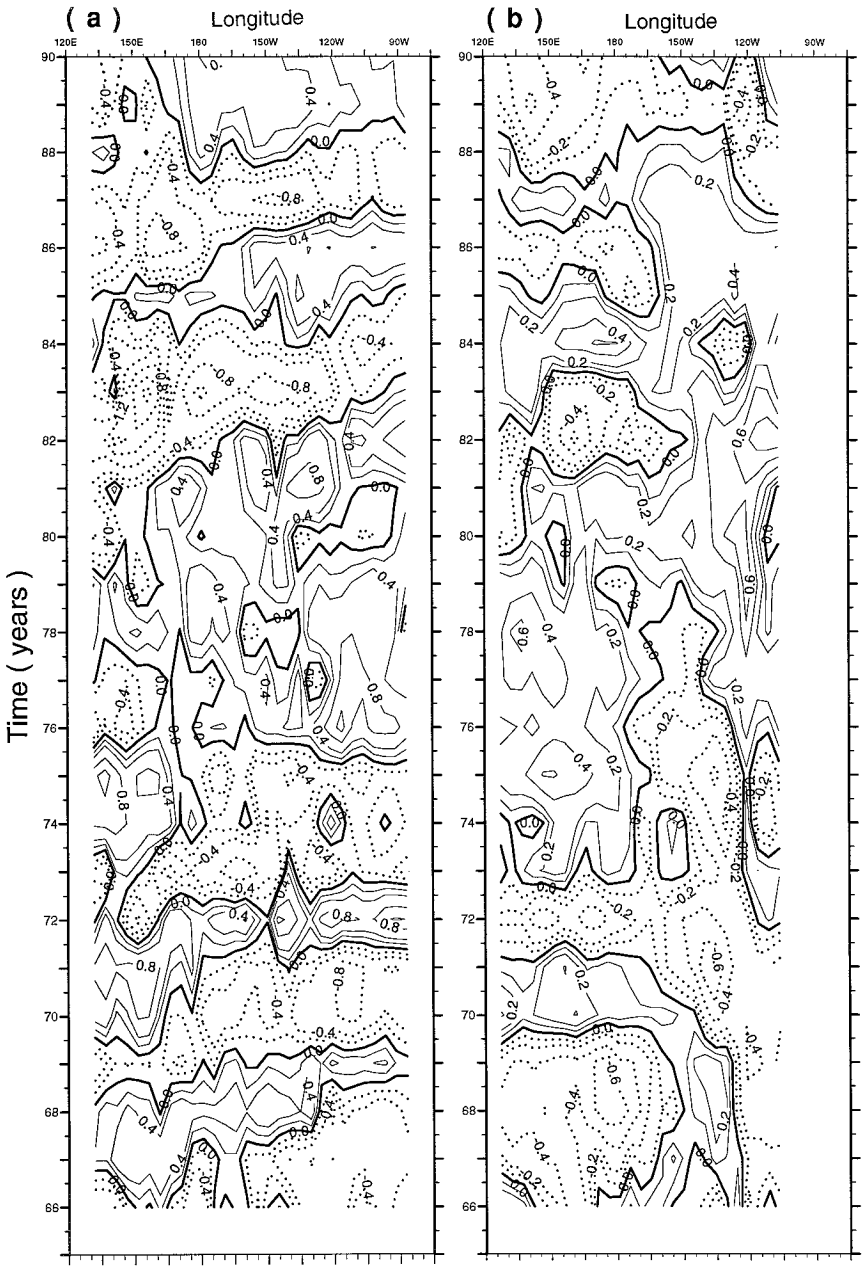

FIG. 3. Interannual variations in heat content (a) along the equator and (b) along 15°N. The contour interval is 0.2°C in both panels, with the dotted line indicating negative values.

Pacific, the El Niño–related anomalies at the subsurface ocean are remarkably large in the western tropical Pacific, as manifested in the 20°C isotherm depth (Fig. 5b), and temperature at 125 m (Fig. 5d). The thermocline displacements have an equatorial maximum in the east and off-equatorial maxima in the tropical western Pacific. Unlike temperature anomalies at the sea surface, those at thermocline depth are large both in the west and in the east, with a prominent seesaw pattern. It is striking that the subsurface temperature anomaly in the central equatorial Pacific Ocean is out of phase with that in the off-equatorial western tropical North Pacific (Fig. 5d). When a positive anomaly occurs in the central equatorial regions, a negative anomaly band tends to occur in the western tropical North Pacific Ocean. In addition, subsurface temperature anomalies in the west exhibit a consistent out-of-phase pattern with those at the sea surface in the central and eastern equatorial Pacific. When SST anomalies are positive in the east, negative temperature anomalies at 125-m depth are large in the western basin, with a maximum off the equator of the tropical North Pacific.

There is a striking contrast of temperature variations

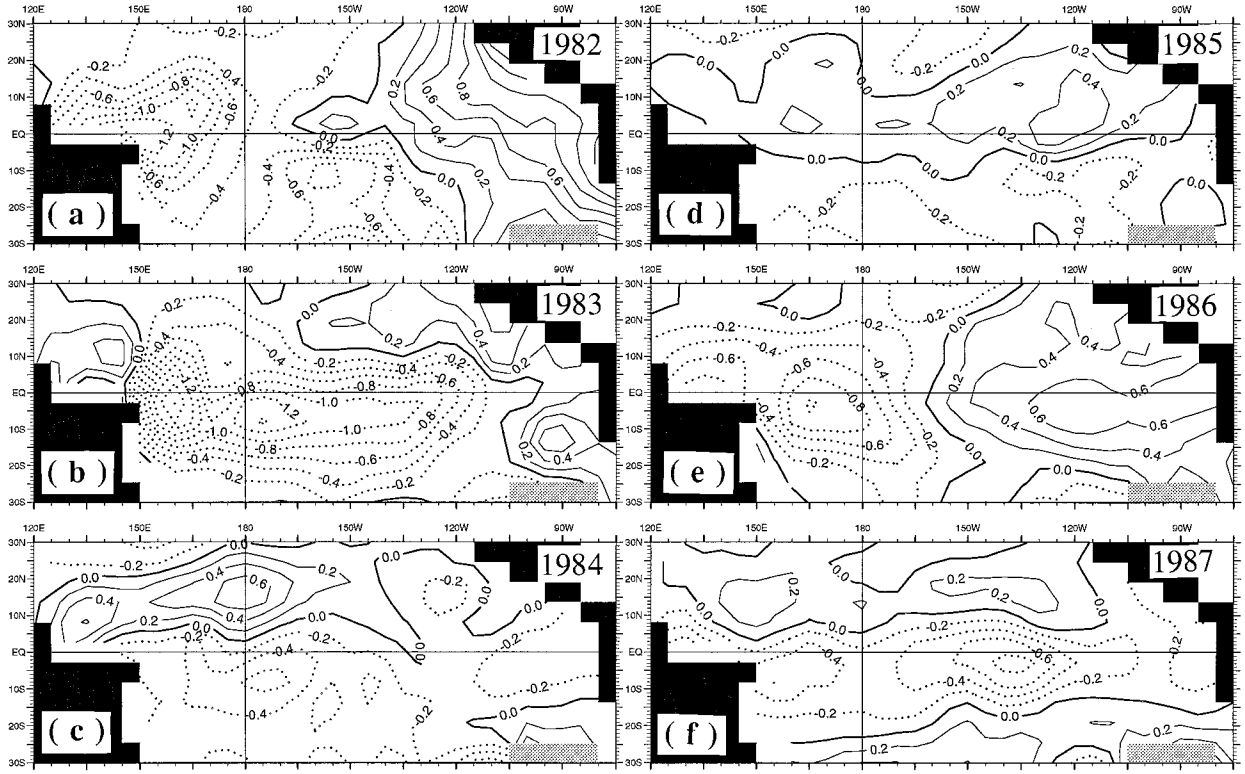

FIG. 4. Horizontal distribution of heat content in the tropical Pacific Ocean for years (a) 1982, (b) 1983, (c) 1984, (d) 1985, (e) 1986, and (f) 1987, respectively. The contour interval is 0.2°C, with the dotted line indicating negative values.

from west to east as a function of depth. This is illustrated by zonal-depth plots of temperature anomalies in Fig. 6a along 7.5°N and Fig. 6b along the equator. During El Niño, a positive temperature anomaly is found in the eastern and central upper ocean with a maximum at about 50-m depth. This is accompanied by a negative anomaly at the subsurface thermocline depth in the west, with the largest anomaly at 100–150-m depth off the equator. Such zonal differences can be more clearly seen in meridional-depth sections of temperature anomalies in the western (152.5°E) and eastern (112.5°W) tropical Pacific (Fig. 7).

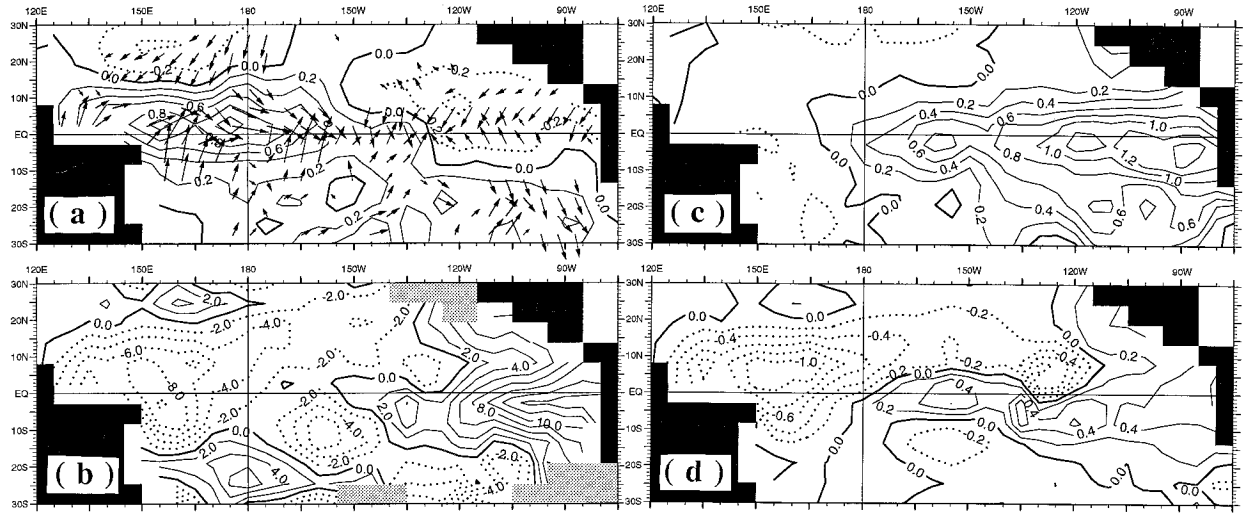

FIG. 5. Composite anomalies of sea surface winds with (a) isoline of the zonal component, (b) the 20°C isotherm depth, (c) SST, and (d) temperature at 125-m depth for an El Niño year. The contour intervals are 0.2 m s^{-1}, 2 m, and 0.2°C, respectively.

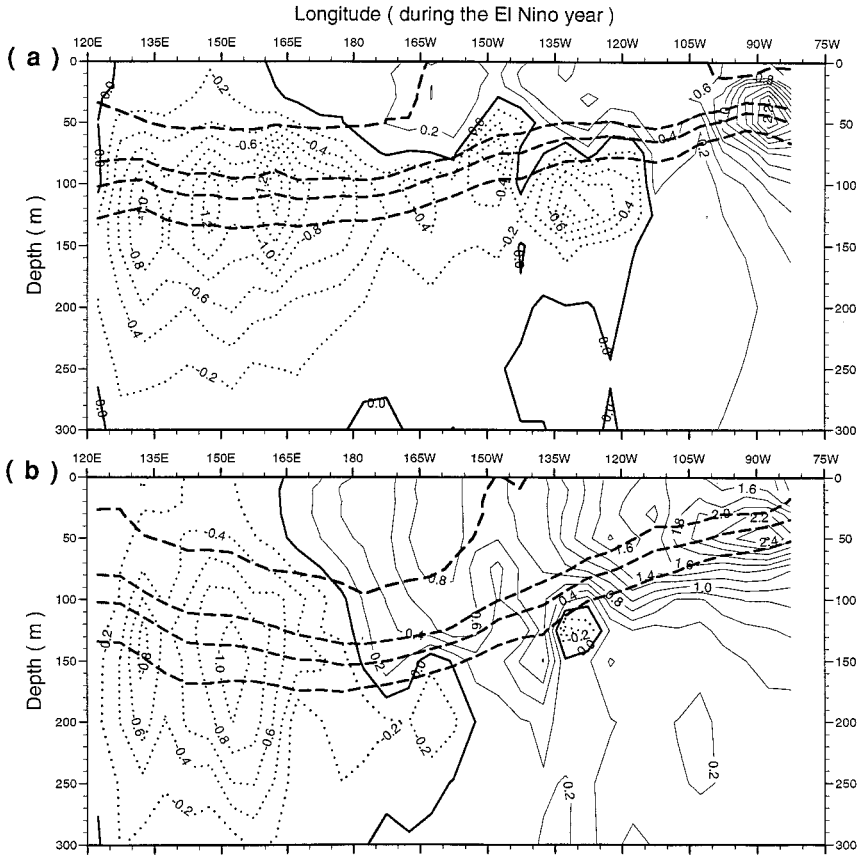

FIG. 6. Zonal-depth sections of composite temperature anomalies (a) along 7.5°N and (b) along the equator for El Niño. The contour interval is 0.2°C, with the dotted line for negative anomalies. The dashed lines show isotherms of 28°, 25°, 23°, and 20°C from above to below, respectively.

During the cold extreme, just as coherent as their warm counterparts, there are also well-organized spatial patterns and phase relationships among atmospheric and oceanic anomaly fields. The La Niña composite anomalies (Fig. 8) exhibit similar spatial patterns but with reversed polarity. Compared to El Niño anomalies, for example, there are opposite changes in the zonal slope of the thermocline, with deepening in the west but shallowing in the east. Correspondingly, the upper-ocean temperature anomalies change sign to become negative in the central and eastern equatorial Pacific, whereas those at the thermocline depth tend to be positive in the western Pacific. The dipole structure of ocean temperature anomalies is evident at subsurface depths (Fig. 8d).

As two extreme phases of the Southern Oscillation, El Niño and La Niña events exhibit revealing structures of atmospheric and oceanic anomaly patterns. Even with yearly anomaly data, our very simple composite fields allow us to document coherent spatial patterns and their contrast between El Niño and La Niña. Nevertheless, as pointed out by many studies, ENSO events take place very irregularly with a timescale of 2–7 yr and usually span 2 calendar years, for example, 1972–73, 1982–83, and 1986–87. There are significant event-to-event differences in spatial structure and evolution as well. These make it difficult to describe structure and evolution by compositing yearly data. However, this choice of compositing periods is imposed on us by the limited data available. The problems could be somewhat mitigated if a typical ENSO year, generally recognized as April to March, or desirably a season or month, rather than a calendar year, is chosen for the averaging period. Alternatively, we will in the following sections use EOFs and lagged correlation analysis to extract the principal structure and to describe typical evolution of the ENSO cycle.

5. EOF analysis for atmospheric and oceanic variables

To detect the dominant structure and time variations of interannual variability, we perform an EOF analysis for various atmospheric and oceanic anomaly fields. The horizontal domain of our analysis is the whole tropical Pacific from 30°N to 30°S. The EOFs are computed based on the correlation coefficient matrix for 1961 to 1990 yearly anomaly fields. Table 1 presents fractional variances for some selected atmospheric and oceanic parameters explained by the first four EOFs.

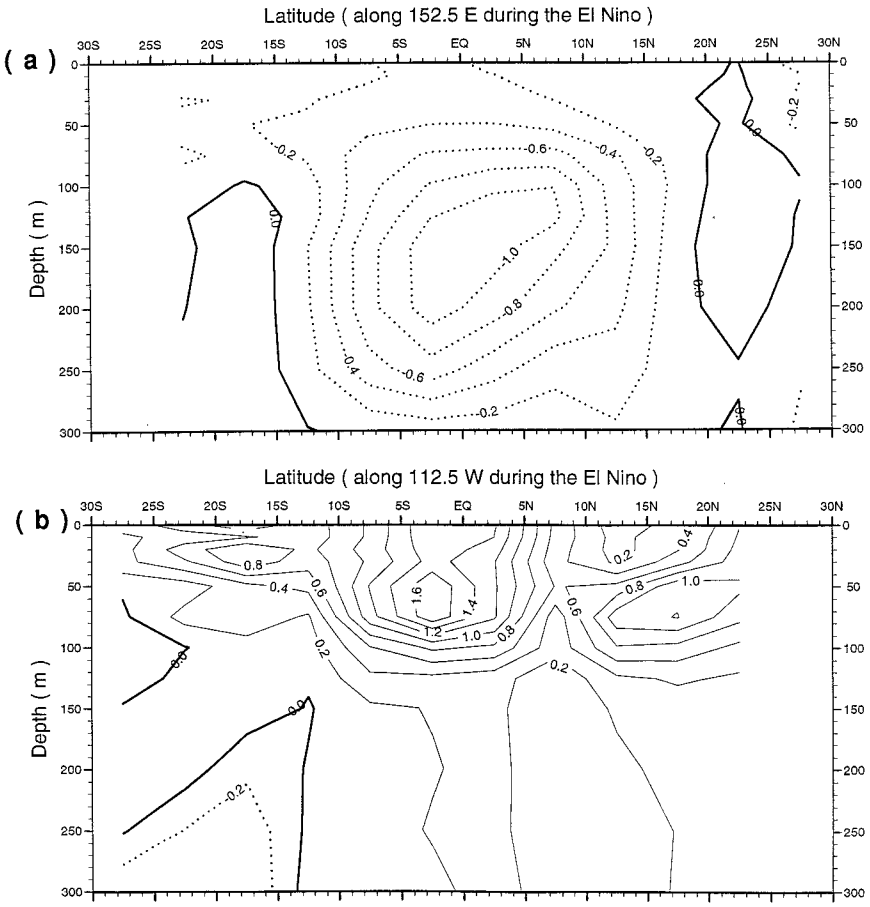

FIG. 7. Meridional-depth sections of temperature anomalies (°C) (a) along 152.5°E and (b) along 112.5°W for an El Niño year.

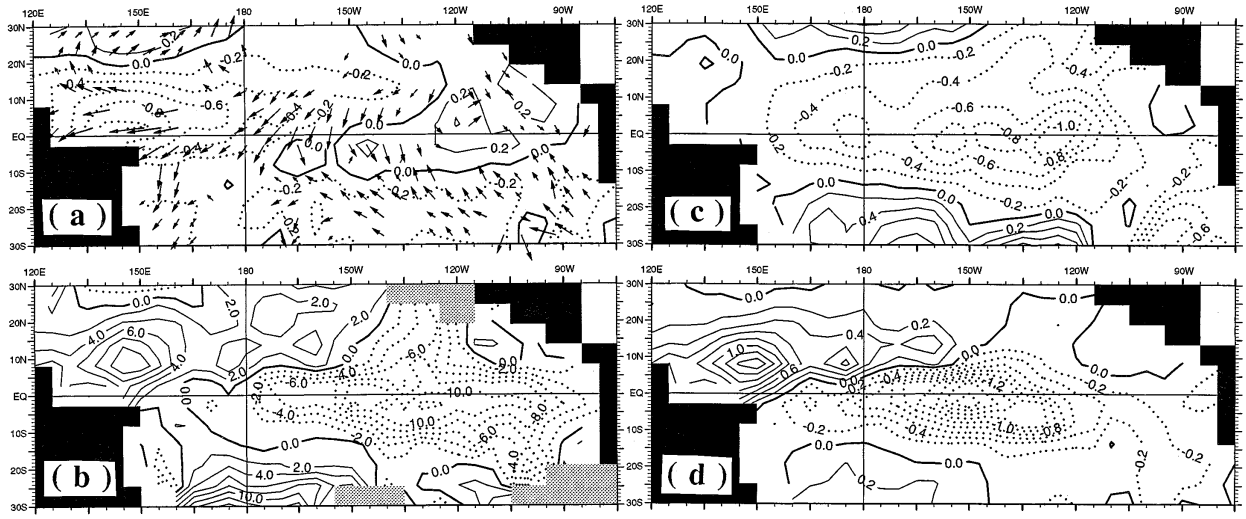

FIG. 8. The same as in Fig. 5 but for La Niña.

TABLE 1. Percentages of variance explained by each of the first four EOF modes for individual atmospheric and oceanic variables [surface winds (combined zonal and meridional components), sea level pressure, the 20°C isotherm depth, sea surface temperature, temperature at 50-, 125-, and 250-m depths, and heat content, respectively].

Variables	Modes (%)				Cumulative
	EOF-1	EOF-2	EOF-3	EOF-4	
Winds (*u*, *v*)	16.7	13.8	7.0	6.0	43.5
SLP	38.8	19.3	6.9	4.2	69.2
20°C	20.3	12.3	11.3	6.3	50.2
SST	20.6	15.6	8.6	5.9	50.7
T (50 m)	21.5	11.5	9.8	5.9	48.7
T (125 m)	18.6	12.6	8.2	7.1	46.5
T (250 m)	14.6	13.5	8.0	7.4	43.5
HC	20.2	12.7	12.0	7.9	52.8

The EOF modes show well-known spatial patterns of various atmospheric and oceanic anomaly fields related with the ENSO phenomenon (figures not given) and resemble results from previous studies. Figure 9 displays the time variations of the first EOF mode for sea surface winds (combined zonal and meridional components), SLP, 20°C isotherm depth, SST, and ocean temperatures at 50-, 125-, and 250-m depths, respectively. It is evident that the first mode corresponds well to El Niño years (e.g., 1972, 1976, 1979, 1982, and 1986) and to La Niña years (e.g., 1971, 1973, 1975, 1984, and 1988). There are concomitant atmospheric and oceanic changes related with the ENSO events. The time series of the first EOF for a given variable is highly correlated with the corresponding time series for all other variables. This is quantitatively illustrated in Table 2, which gives the matrix of simultaneous correlation coefficients between the temporal coefficients for the first EOF mode of a certain variable and the corre-

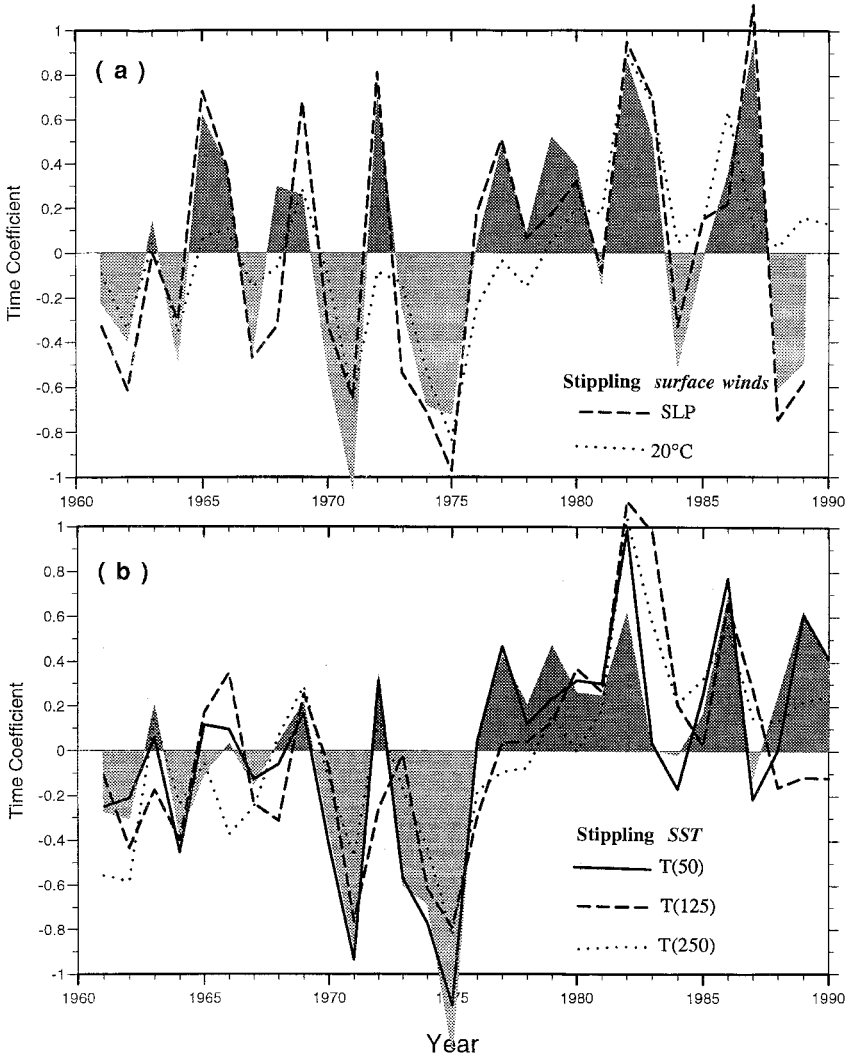

FIG. 9. Time variations of the first EOF mode for sea surface winds (stippling), SLP (dashed line), and the 20°C isotherm depth (dotted line) in (a); and for SST (stippling) and temperature at depths of 50 m (solid line), 125 m (dashed line), and 250 m (dotted line) in (b), respectively.

TABLE 2. Matrix of correlation coefficients between the time variations of the first EOF for different atmospheric and oceanic variables. The table gives the values multiplied by 100.

	Winds (u, v)	SLP	20°C	SST	T (50 m)	T (125 m)	T (250 m)	HC
Winds (u, v)	100	92	67	61	66	69	58	73
SLP		100	66	55	61	71	60	73
20°C			100	78	82	94	90	96
SST				100	96	63	77	87
T (50 m)					100	69	77	92
T (125 m)						100	79	88
T (250 m)							100	91
HC								100

sponding time coefficients of another variable. Thus, not only do variables within the atmosphere or within the ocean exhibit coherent phase relationships, but different oceanic and atmospheric fields are linked to each other. In addition to these ENSO-related interannual variations, decade-scale changes can also be seen. In particular, the individual warm and cold events appear to be modulated by a low-frequency fluctuation with a timescale of 5–8 yr. For example, it is evident that there is a cooling period between 1969 and 1976, with strong easterly wind and deep thermocline in the west (Figs. 2–3).

6. Space–time evolution: A correlation analysis

Section 3 presented some characteristic features of the interannual variations in atmospheric and oceanic anomaly fields. In view of the multitude of warm and cold events appearing during the analysis periods, we now present results of correlation analysis to more clearly describe the most recurrent space–time evolution of coupled oceanic and atmospheric anomaly fields during an ENSO cycle.

To describe space–time evolution, we perform time-lag correlation analyses on the combined oceanic and atmospheric anomaly data. Since variations in SLP indicate very well the interannual variations associated with El Niño and La Niña events, and exhibit the largest variance explained by the first EOF mode (Table 1), we choose the temporal coefficients of the first SLP EOF mode (dashed line in Fig. 9a) as reference time for defining time evolution of the interannual variations. Additional comparison of these time series with SO index, a commonly used indicator of the tropical interannual variability, shows good agreement. Then, temporal correlation coefficients are computed between this reference time and the anomaly fields at individual grid points for different time lags, as shown in Figs. 10 and 11. The panels have been arranged in the order of increasing time lags with 1-yr interval. For example, Fig. 11c illustrates

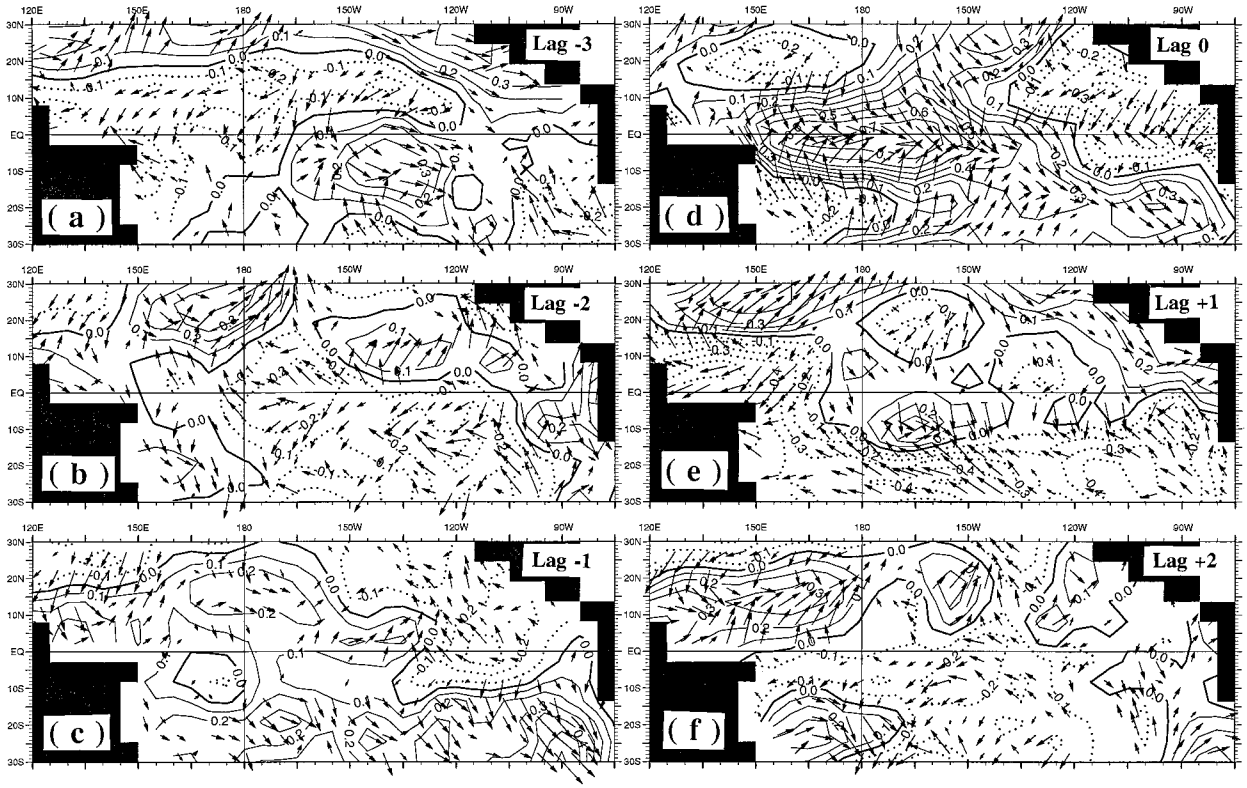

FIG. 10. Distributions of the correlation coefficients between the time variations of the first SLP EOF and surface winds, with the time variations lagging the gridpoint data by (a) 3 yr, (b) 2 yr, (c) 1 yr, and (d) 0 yr, and with the time variations leading the gridpoint data by (e) 1 yr and (f) 2 yr, respectively. The contour interval is 0.1, with the dotted line for negative areas.

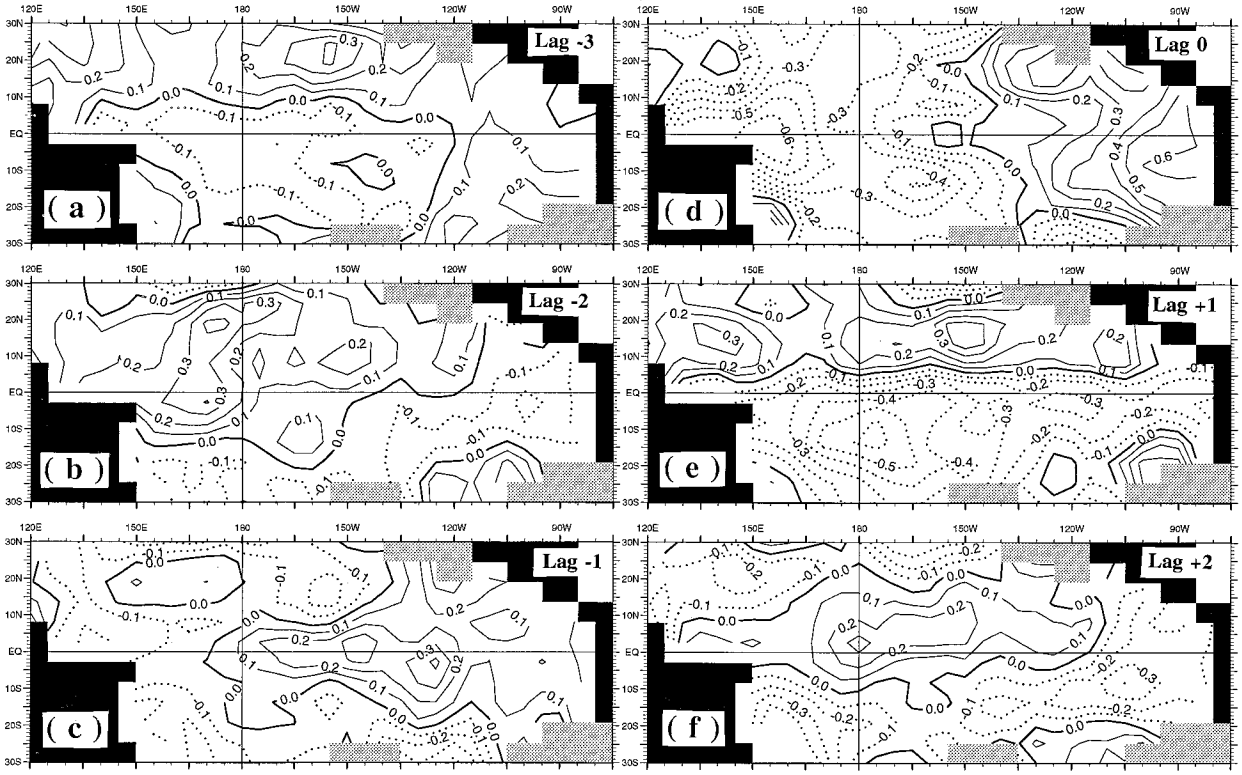

FIG. 11. The same as in Fig. 10 but for heat content.

the results for the reference time lagging heat content by 1 yr, and Fig. 11d shows the correlation values for the reference time leading the data by 1 yr, and so on.

Figure 10 presents space–time evolution for the surface winds during 6 successive years. The sequence depicts the dominant surface wind anomaly patterns at 1-yr intervals through the ENSO cycle. The anomaly patterns at zero time lag correspond to El Niño (warm) phase, those at lag +2 yr approximately coincide with La Niña (cold) phase, and those at lag +1 yr represent the transitional state. Note some similarity, as expected, in spatial structure between Figs. 10b and 10f and between Figs. 10a and 10e, respectively.

At lag −3 yr (Fig. 10a), easterly wind anomalies prevail over the western and central tropical North Pacific along 10°N; to the east and south, there are westerly wind anomalies with maxima over the central South Pacific along 10°S. In the western North Pacific along the Asian coast, there is an enhanced anticyclonic surface circulation. Two years before the warm phase (Fig. 10b), that is, corresponding approximately to the cold phase, there is an intensification of the trade winds in the central equatorial Pacific and anomalous off-equatorward flow over the eastern and central equatorial regions. Note that there is enhanced cyclonic surface circulation in the western North Pacific near the date line. One year prior to the warm phase, at lag −1 yr (Fig. 10c), the easterly wind anomalies in the central equatorial Pacific become weaker and are confined to the eastern North Pacific. Westerly wind anomalies have developed in the Tropics west of the date line with cyclonic circulation over the northwestern Pacific. In the South Pacific, the surface wind shows a general pattern of westerly to northwesterly anomalous flow across most of the basin south of 10°S, reflecting a diminution of the southeast trade winds. During the warm phase near zero time lag (Fig. 10d), westerly anomalies that appeared just west of the date line (Fig. 10c) now have strengthened and spread eastward to cover a vast area of the western and central equatorial Pacific, accompanied by an anomalous equatorward-directed flow across the central equatorial Pacific in both hemispheres. There is an anomalous northerly flow across the normal position of the ITCZ in the tropical northeastern Pacific, manifesting a southward shift of the ITCZ. These surface wind anomalies generally reflect the weakening of the anticyclone over the southeastern Pacific and thus the weakening of the equatorial easterly trade winds. In addition, there is an enhanced anticyclonic surface circulation in the western tropical North Pacific. One year later after the warm phase (Fig. 10e), the anomalous equatorial westerlies weaken and then reverse in the western Pacific. Another striking feature is an anomalous anticyclonic circulation developing off the equatorial region in the western tropical North Pacific. Next, easterly wind anomalies begin to occur in the Tropics.

Two years after the warm phase (Fig. 10f), weak easterly wind anomalies are found over much of the ocean basin, with significant anomalous cyclonic flows in the tropical northwestern Pacific west of the date line.

The dominant anomaly patterns of temporal evolution for SST are similar to those described in previous studies (Rasmusson and Carpenter 1982; Wright and Wallace 1988). We describe the SST variability in brief so we can make comparisons with the subsurface changes. Two years before the warm phase—that is, corresponding approximately to the cold phase—negative SST anomalies cover the eastern equatorial Pacific and South American coast, whereas positive SST anomalies are found in the central and western Pacific, but characterized by small amplitudes. At lag −1 yr, the negative SST anomalies have disappeared in the east and are replaced by positive anomalies to the east of the date line. The positive anomalies have also disappeared from the region west of the date line. During the warm phase near zero time lag, large positive SST anomalies now cover a large part region of the central and eastern Pacific, with negative SST anomalies to the west. One year after the warm phase, the anomaly patterns are almost reversed. Negative SST anomalies reappear in the eastern equatorial Pacific and southern American coast.

The structure and evolution of subsurface temperature anomalies are strikingly different from those at the sea surface. Figure 11 presents the states of the space–time evolution for heat content during 6 successive years. Structural contrasts in longitude from west to east, and in latitude from on the equator to off the equator are clearly evident during the ENSO evolution. The typical space–time evolution of heat content is characterized by a systematic eastward anomaly movement along the equator, and a westward movement off the equator in the tropical North Pacific. Figure 11d shows the horizontal distribution of the correlation coefficients at zero time lag, corresponding to an El Niño state. There is an east–west seesaw pattern characterized by an increase of heat content in the east, and a decrease in the western and central Pacific. The positive anomaly can be continuously traced back to the western and central equatorial Pacific 1 yr before (Fig. 11c), and farther back to the off-equatorial region of the tropical North Pacific at lag −2 yr (Fig. 11b) and to the tropical northeastern and coastal Pacific at lag −3 years (Fig. 11a). Also, the negative anomaly in Fig. 11d can be traced back to Fig. 11a. Subsequently, heat content anomalies continue to move eastward along the equator and westward off the equator. One year after the El Niño phase (Fig. 11e), positive anomalies are now found in the off-equatorial tropical North Pacific and negative anomalies cover the entire equatorial regions. There is a striking north–south contrast of the anomaly pattern, with decrease of heat content at all longitude in the equatorial region but increase in the off-equatorial North Pacific of 10°–20°N latitudes. By lag +2 yr (Fig. 11f), the positive anomalies are located in the western and central equatorial Pacific while the negative anomalies are found in the eastern Pacific. This spatial structure is similar to that at lag −2 yr (Fig. 11b) and corresponds to the La Niña state.

Phase propagation features are further illustrated by showing the corresponding longitude–time distribution of the lagged correlation coefficients along the equator and along 15°N. The SLP anomalies show the signature of eastward phase propagation both along the equator (Fig. 12a) and off the equator of the tropical North Pacific (Fig. 12b). In contrast, surface zonal winds along the equator (Fig. 12c) do not show such systematic phase propagation, indicating a dominant standing pattern. In the ocean, phase propagation of thermal anomalies is evident below the sea surface with no evidence for propagation of SST anomalies (Fig. 12d).

At subsurface depths, coherent anomaly movement can be clearly seen (Zhang and Levitus 1996). The longitude–time distribution of the correlation coefficients reveals an eastward phase propagation along the equator and westward off the equator in the northern tropical Pacific. Furthermore, the correlation coefficients suggest sequential connections between variations on and off the equator of the tropical North Pacific through the western and eastern boundary regions. The possible phase connections in a circuit around the equatorial and tropical North Pacific are illustrated in Fig. 13 for heat content along 15°N, 152.5°E, the equator, and 102.5°W, respectively. It is evident that there is a slow propagation of the anomaly from west to east along the equator, from east to west off the equator, and in the western and eastern boundary regions. At lag −2 yr, that is, 2 yr before the El Niño warm SST in the east, there are large positive heat content anomalies in the western Pacific (Fig. 13c), which can be traced back to the western boundary regions (Fig. 13b) and to the off-equatorial North Pacific along 15°N (Fig. 13a). The positive anomalies move eastward along the equator and take about 2 yr to cross the basin (Fig. 13c). Their arrival at the central and eastern equatorial Pacific Ocean results in warming at the sea surface (Fig. 12d). Then these anomalies continue their phase movement northward along the eastern boundary (Fig. 13d) and, subsequently, westward off the equator of the tropical North Pacific along 15°N (Fig. 13a), reaching the western Pacific regions at lag +1 yr. Finally, they extend southward into the equatorial waveguide (Fig. 13b) and move again eastward along the equator, completing one cycle. Meanwhile, at lag 0 yr (Fig. 13c), there are negative heat content anomalies in the western Pacific, which can also be continuously traced back to the western boundaries (Fig. 13b) and to the off-equatorial tropical North Pacific (Fig. 13a). These negative anomalies also move eastward along the equator and arrive in the eastern Pacific at lag +2 yr, resulting in phase reversal there. They then continue their northward movement along the North American coast. Therefore, ENSO evolution involves coherent and consistent anomaly movement and phase transition in the subsurface ocean from west to east along

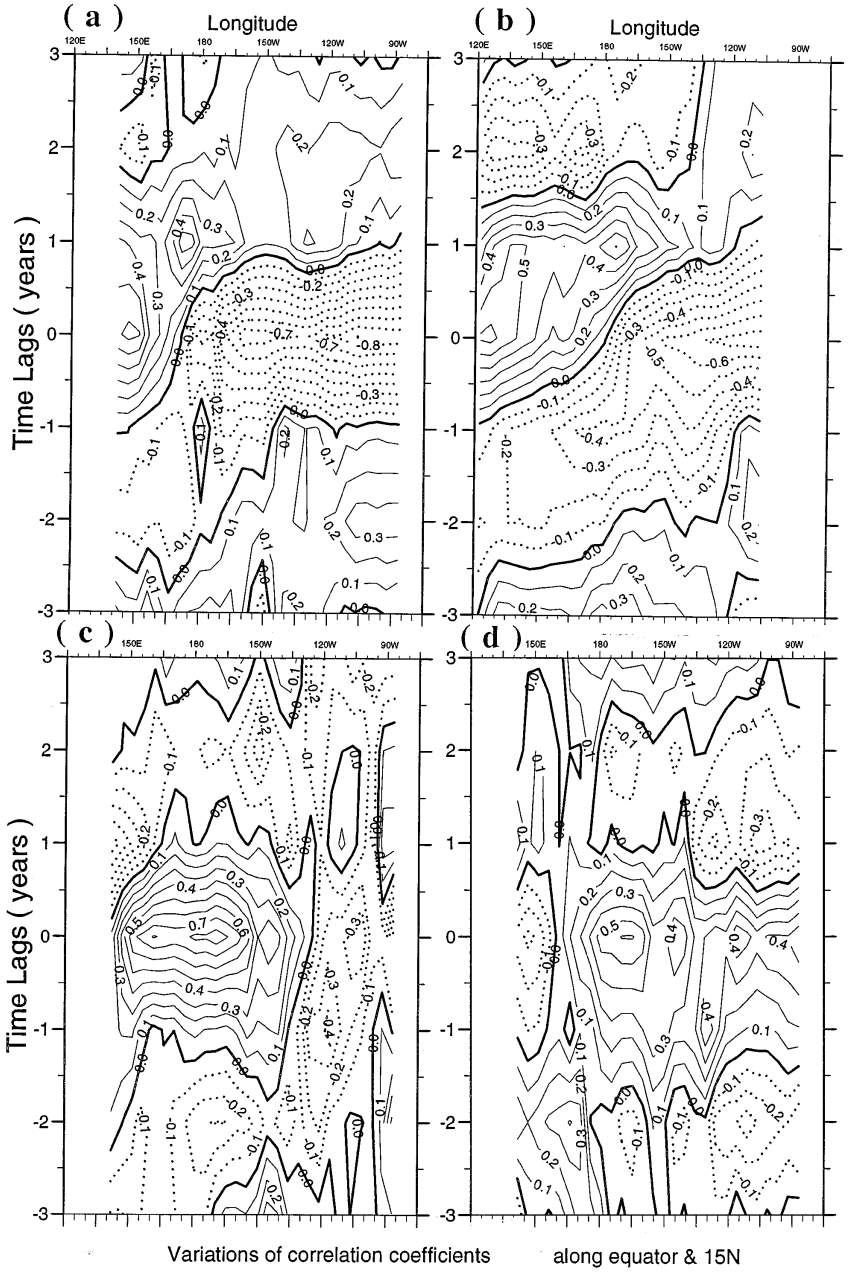

FIG. 12. Temporal variations of the correlation coefficients for SLP (a) along the equator and (b) along 15°N, and for (c) surface zonal winds and (d) SST along the equator. The contour interval is 0.1, with the dotted line for negative correlation.

the equator, from on the equator to off the equator of the tropical North Pacific in the eastern boundary, and then from east to west off the equator and back to equatorial regions in the western boundary, suggesting a cycle.

There are clear phase relations in SST and subsurface thermal anomalies, as evident in the original data plot (Figs. 2b and 3) and the correlation analyses (Figs. 12d and 13). Variations at subsurface depths in the western equatorial Pacific lead SST variations in the eastern equatorial Pacific by about 2 yr. Because of upward slope of the tropical thermocline from west to east, an eastward movement of subsurface thermal anomalies from west along the equator produces SST anomalies in the central and eastern equatorial Pacific, causing a transition from one phase to another. For example, 2 yr before an eastern tropical Pacific surface warming, a cold condition prevails at the sea surface in the east (i.e., La Niña condition). At this time, there are positive subsurface anomalies in the western tropical Pacific, which propagate eastward along the equator. About 2

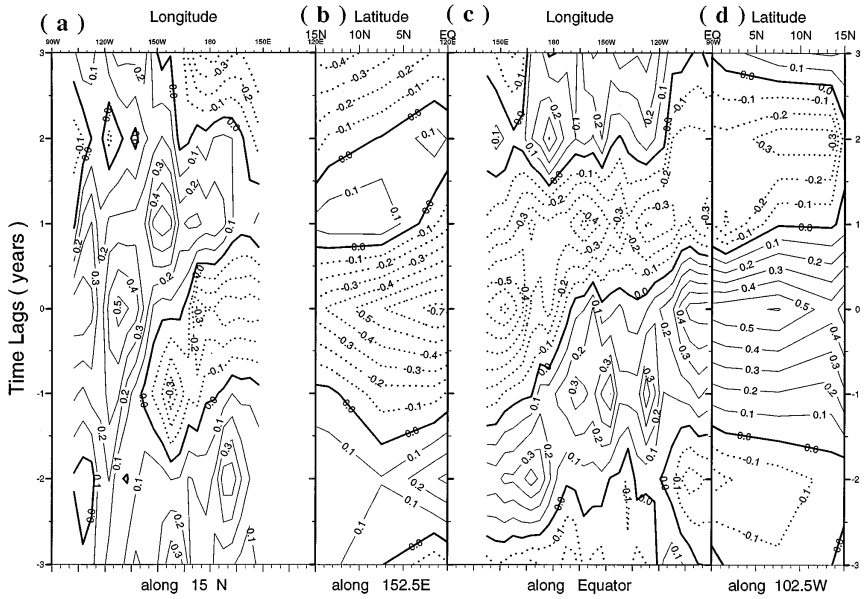

FIG. 13. Temporal variations of the correlation coefficients of heat content on a circuit around the northern tropical Pacific: (a) zonal section along 15°N, (b) meridional section along 152.5°E, (c) zonal section along the equator, and (d) meridional section along 102.5°W. Note the east to west shift in longitude in the two zonal sections [(a) and (c)] and the north to south shift in latitude in the two meridional sections [(b) and (d)] in order to form a continuous circuit at their intersection.

yr later, their arrival at the eastern equatorial Pacific, consequently, results in warm SST in the east, thus introducing a phase transition into El Niño in the tropical Pacific. At the same time, subsurface negative anomalies, after their movement across the tropical North Pacific, are just located in the western equatorial Pacific. Subsequently, they move eastward along the equator. About 2 yr later, their arrival in the eastern equatorial Pacific causes cold SST and a La Niña condition appears in the tropical Pacific.

The relation between heat content and surface winds is also evident. One year before the El Niño (Fig. 10c), there appears an anomalous cyclonic circulation flow in the off-equatorial northwestern Pacific region, which reinforces the shoaling of the thermocline in the west. During an El Niño year with westerly wind anomalies over the central and western equatorial Pacific (Fig. 10d), the spatial distribution of heat content is characterized by an increase in the east but a decrease in the western and central tropical Pacific (Fig. 11d). At the same time, an anomalous anticyclonic circulation is found in the tropical northwestern Pacific, which favors the deepening of the thermocline in the off-equatorial tropical North Pacific. The striking feature at lag +1 yr, one year after El Niño, is an appearance of strong anticyclonic circulation anomalies in the off-equatorial North Pacific west of the date line (Fig. 10e). This coincides with an increase of the off-equatorial heat content in the tropical North Pacific at all longitudes, at the expense of heat content in the entire equatorial regions (Fig. 11e). Next, an opposite pattern to El Niño is observed during La Niña (Figs. 10f and 11f, or Figs. 11b and 12b).

In summary, there are coherent patterns in the atmosphere and in the ocean during the ENSO cycle, characterized by a slow phase propagation of subsurface thermal anomalies around the tropical Pacific basin, which indicates a nonequilibrium response of the ocean to early atmospheric forcing. This subsurface anomaly evolution has coherent phase relations with SST and surface winds. The onset of El Niño is characterized by an appearance of subsurface thermal anomalies in the western Pacific Ocean, which propagate systematically eastward along the equator. Their arrival in the east results in reversal of SST anomaly polarity, which then produces correspondingly surface wind anomalies in the west, which in turn produce and intensify the subsurface anomalies off the equator, thus terminating one phase of the Southern Oscillation. At the same time, the continual anomaly movement at depths from east to west off the equator provides a phase transition mechanism back to the west. In due course, opposite anomalies are located in the equatorial western Pacific at subsurface depths, introducing an opposite SO phase and beginning a new cycle. It appears that interannual variability in the tropical Pacific represents a slowly evolving air–sea coupled mode.

7. An evaluation of ENSO theories and models

In the past decades, theoretical studies, observational analyses, and numerical simulations have been con-

ducted extensively and intensively to describe and understand the ENSO phenomenon. No single theory exists for ENSO at present. Many ocean and coupled atmosphere–ocean models have been developed. However, there are considerable discrepancies in comparison of simulations with the corresponding observations. In addition various coupled models behave differently (Philander et al. 1989; Neelin and Latif 1992). The data analyses presented in this paper, particularly at subsurface depths, provide an observational basis for the study of space–time evolution of the coupled tropical Pacific atmosphere–ocean system.

Two theories have been put forward to explain the El Niño dynamics and its interannual cycle in the tropical Pacific climate system. One is known as the ''buildup'' of warm waters (i.e., deep thermocline) in the western equatorial Pacific Ocean by stronger-than-normal trade winds for a year or more (Wyrtki 1975). The onset of El Niño is accompanied by discharge of the stored warm waters to the central and eastern Pacific, and further to higher latitudes (Cane et al. 1986; Springer et al. 1990). The timescale of the ENSO cycle is attributed to a slow recharging of the warm water reservoir, characterized by deepening of the thermocline in the west. Our observational analyses based on the basinwide upper-ocean thermal data suggest two discrepancies with the buildup hypothesis. The first is the spatial scale of interannual variability at subsurface depths during the ENSO cycle. The El Niño year is characterized by an east–west seesaw pattern, with positive anomalies in the east and negative anomalies in the west (Fig. 11d). One year later, there is a striking contrast of equatorial and off-equatorial variations, with east–west oriented bands in longitude (Fig. 11e). This means that following El Niño, there is a systematic heat gain in the off-equatorial tropical Pacific centered around 15°N, whereas there is a heat loss confined to a fairly narrow band of the equatorial regions and to the tropical South Pacific. Thus, the buildup and release of the equatorial heat content in the tropical North Pacific occurs in a much narrower band than inferred by Wyrtki (1985). Our subsurface data analyses are consistent with the analyses of sea level and modeling results given by Springer et al. (1990). Based on their observational analysis of the 1991–93 El Niño, Kessler and McPhaden (1995) have pointed out the second discrepancy between data and the theory that requires a buildup of a thick warm layer (deep thermocline) in the west prior to an El Niño event. The zonal structure and time evolution of heat content along the equator (Fig. 3) demonstrate the existence of two signals, interannual and interdecadal variability. During the period 1969–75, the equatorial thermocline is deep in the west but shallow in the east. In contrast, during the 1980s the equatorial thermocline is shallow in the west but deep in the east. There is, however, frequent occurrence of warm SO phase during this period, including the strongest El Niño event (1982–83) of the century. This suggests that a deep equatorial thermocline in the western Pacific Ocean is not a prerequisite for the occurrence of El Niño.

Another theory of the ENSO cycle is the delayed oscillator mechanism. This theory emphasizes equatorial wave dynamics, characterized by explicit Kelvin waves, which propagate eastward along the equator; the first meridional Rossby wave, which propagates westward; and its reflection at the low latitude western boundary. The phase reversal is provided by the equatorial Rossby wave, which is generated at the height of the ENSO event in the midbasin and propagates to the western boundary and then reflects to return along the equator as the equatorial Kelvin wave. The slow interannual timescale of the ENSO evolution as observed, which cannot be accounted for by these intraseasonal equatorial waves alone, is attributed to coupled local air–sea instability in the midbasin. Although this theory can partly explain ENSO, it does not explain the onset phase well. Furthermore, numerous studies have shown significant discrepancies and suggest a need for its modification (Philander et al. 1992; Chao and Philander 1993; Levitus et al. 1994b; Kessler and McPhaden 1995; Picaut and Delcroix 1995; Boulanger and Menkes 1995; Zhang and Levitus 1996). Our analyses provide new information about subsurface ocean variability associated with ENSO. For example, our data analyses clearly indicate that interannual variations involve the entire tropical Pacific basin, not only the equatorial region but also the off-equatorial tropical North Pacific at latitudes of 10°–20°N where large signals are observed at subsurface depths during the entire ENSO cycle (Fig. 11). The coherent anomaly patterns in the atmosphere as well as the ocean indicate that air–sea interactions occur on the basin scale, including the western tropical North Pacific where there is a striking anticyclonic circulation 1 yr after an El Niño (Fig. 10e). Second, it appears that interannual variability represents a slowly evolving air–sea coupled mode, rather than individual free oceanic Rossby and Kelvin wave modes. Third, there is evidence of continual phase propagation at subsurface depths on and off the equator, with apparent continuity of equatorial signals and off-equatorial anomalies both in the western and eastern boundaries. Therefore, the basinwide subsurface phase propagation on interannual timescales would be a more fundamental mechanism working in the real world system. These preferential, relatively slow modes of propagation of subsurface temperature anomalies cause phase transitions at the sea surface in the east but at depth in the west, providing a transition mechanism from one SO phase to another. Their cycling time around the tropical Pacific basin may determine the period of the El Niño occurrence.

Next, we turn to model simulations of interannual variability in the tropical Pacific climate system. Several ocean and coupled atmosphere–ocean models have been developed with the ability to produce interannual variability, but they differ strikingly from each other, especially in their evolutionary behavior (Philander et al.

1989; Neelin et al. 1992). It follows that dominant mechanisms responsible for tropical interannual variability are different in different models and may be also different from those in the real system (e.g., Cane and Zebiak 1985; Schopf and Suarez 1988; Lau et al. 1992; Philander et al. 1992; Nagai et al. 1992; Latif et al. 1993; Chao and Philander 1993). The main differences appear to be phase propagation and relationship between anomalies in the ocean and atmosphere. The interannual thermal variability in the tropical Pacific Ocean described by Philander et al. (1992) and Chao and Philander (1993) bears a close resemblance to our data analyses, such as the phase propagation of subsurface thermal pattern, a suggestion of spatial inhomogeneities of phase speed, and phase differences between SST and subsurface thermal variations. It is also evident that there are some discrepancies as compared with our observations. For example, the off-equatorial anomaly centers at subsurface depths in the model are not displaced as far northward as are the observational data. Since the model thermocline is rather weak and diffuse, there is noticeable underestimation of subsurface thermal variability around the entire basin, particularly in the northeastern tropical Pacific compared to observations. Consequently, the continual phase propagation around the tropical basin observed in the data is less coherent in the model. Instead, the subsurface anomalies associated with El Niño and La Niña events in the model are likely to be locally forced around the dateline and subsequently propagate westward as low-latitude Rossby waves, whereas the observed data suggest that subsurface anomalies reaching the western boundary have their origin in the eastern boundary and their westward propagation provides a phase transition mechanism in the western Pacific.

The other ocean or coupled models with low resolution seem to have problems in realistically producing the subsurface phase propagation in the tropical Pacific basin (e.g., Lau et al. 1992). These models do not resolve adequately the seesaw anomaly pattern on and off equator at subsurface depths. They underestimate or even lack the important phase differences in interannual thermal variations at the sea surface and at subsurface depths. Instead, the interannual variations are dominated by local air–sea interactions, which are characterized by pronounced westward phase propagation and phase differences between variations in SST and surface winds. Without a phase-switching mechanism provided by subsurface ocean dynamics, interannual variability in these models is a westward-propagating mode as discussed by Hirst (1986) and Neelin (1990), and, therefore, is strikingly different from our data analyses.

In addition to interannual fluctuations, there is clear evidence for decadal variations in the coupled tropical Pacific climate system (Fig. 9). At subsurface ocean depths, the appearance of warm and cold events is quite regular during the periods 1966–76 and 1980–88, with clear eastward propagation along the equator and westward propagation off the equator (Fig. 3). During the period 1976–82, the tropical Pacific Ocean is anomalously warm and the phase propagation is interrupted, suggesting that decadal processes can change some features of interannual variability. No theory explains this decadal ENSO variability and current numerical models are unable to realistically simulate it either.

8. Summary

Based on observational data, we described the spatial structure and time evolution of interannual variability of the coupled tropical Pacific climate system, with emphasis on subsurface ocean thermal anomalies. Because of data sampling limitations, our results must be viewed with some caution. An obvious weakness of the paper is the use of calendar year averages, particularly considering the fact that ENSO events occur very irregularly and usually span 2 calendar years with event-to-event differences. We hope to resolve this problem by working with seasonal datasets when more data are available in the future. Results from the IOC/GODAR project indicate that there will be some increase of historical data for this region (Levitus et al. 1994c).

Our simple composites describe the characteristic anomaly patterns of the warm and cold extremes of the SO (El Niño and La Niña). Time evolution of ocean thermal anomalies is examined using a lagged correlation analysis. There are well-defined three-dimensional patterns and phase relationships between atmospheric and oceanic anomalies, showing coherent variations from the western warm pool region to cold eastern Pacific, from subsurface to surface, and from the equatorial waveguide to off-equatorial region of the tropical North Pacific Ocean. During an El Niño year, a positive temperature anomaly is found in the eastern and central tropical upper ocean with a maximum located at about 50-m depth on the equator. This is accompanied by a negative temperature anomaly in the western Pacific subsurface ocean with the largest anomaly located at the thermocline depth off the equator. The spatial pattern of atmospheric and oceanic anomaly fields is in the opposite situation during La Niña.

One of the most interesting results in this work is the very slow (interannual) continual propagation of subsurface thermal anomalies during an El Niño cycle around the tropical Pacific basin, eastward on the equator but westward in the tropical North Pacific regions, and their apparent phase continuity at the western and eastern boundaries. Furthermore, these subsurface anomalies are shown to have consistent and coherent phase relations with variations in SST and surface winds. Subsurface propagation of thermal anomalies on the interannual timescale causes phase transition at the sea surface in the central and eastern equatorial Pacific and at depths in the western Pacific. The altered SST induces variations in the surface winds, which in turn feed back to the ocean. It is the coupled interactions

between SST, surface winds, and the ocean thermocline that give rise to coherent propagation of subsurface anomaly patterns. Therefore, the coherent anomaly patterns on the basin scale, although manifested at subsurface ocean depths, represent a coupled phenomenon between the atmosphere and ocean. The continual phase propagation of subsurface thermal anomalies in succession around the entire tropical Pacific would seem to play a centrally important role in interannual variability in the system.

Based on our results, the ENSO evolution can be summarized as follows. The principal elements of the ENSO cycle include continual anomaly movement at subsurface depths, a phase transition mechanism for SST, and then coherent air–sea interactions. Unique structure and phase propagation of thermal anomalies at subsurface depths, and its relation to surface winds and SST determine the nature of interannual variability. Beginning with warm phase of the SO (i.e., El Niño), positive SST anomalies cover the central and eastern tropical Pacific Ocean, and are accompanied by westerly wind anomalies over the western and central equatorial Pacific. At subsurface ocean depths, thermal anomalies are characterized by an east–west seesaw pattern, with shoaling of the thermocline in the west but deepening in the east. Correspondingly, there are significant negative temperature anomalies at subsurface depths in the western Pacific Ocean, which are out of phase with those in the east. If all components in the system are in equilibrium with each other, these El Niño conditions would have been maintained to persist by local air–sea interactions. The subsurface ocean, however, is not in temporal equilibrium with the atmospheric forcing. Instead, there is systematic and coherent phase propagation: eastward along the equator and westward off the equator. The subsurface negative anomalies in the west take about 2 yr to cross the equatorial basin. Because of the sloping thermocline along the equator, their arrival results in negative SST anomalies in the east, which in turn introduce the corresponding in-phase response of atmospheric surface winds, characterized by easterly wind anomalies in the western and central equatorial Pacific, thus terminating El Niño conditions. At the same time, the subsurface ocean still continues its nonequilibrium adjustment on and off the equator. The subsurface positive anomalies located in the east during El Niño move northward along the North American coast, and then propagate westward off the equator across the tropical North Pacific, and finally extend equatorward into the equatorial waveguide in the west. Thus, in due course, La Niña conditions develop and prevail in the tropical Pacific, characterized by, among others, significant negative temperature anomalies at subsurface depths in the western tropical Pacific. The subsequent evolution follows the same route but with reverse polarity, completing an ENSO cycle.

Our description of the basinwide structure and time evolution of interannual subsurface ocean variability is based on historical observational data that have only recently become available in digital form. These results have dynamical implications that will help to improve our understanding of interannual variability of the tropical climate system. The data analyses clearly show the important role of subsurface anomaly movement and phase transition during the ENSO cycle. In particular, the space–time evolution of the subsurface ocean thermal anomalies appears to be in the form of a cycle on interannual timescale around the basin, showing coherent anomaly movement: eastward along the equator but westward off the equator of the tropical North Pacific. During El Niño, the seeds for La Niña are already present to the west of El Niño conditions at subsurface depths in the western tropical Pacific where there are significant negative temperature anomalies, which in turn can be traced back to the off-equatorial central and eastern tropical North Pacific, and farther to the eastern equatorial regions. Subsequently, the subsurface negative anomalies expand and propagate eastward along the equatorial thermocline. Its arrival causes the termination of the El Niño surface conditions in the eastern Pacific where the La Niña conditions prevail thereafter. Note that, unlike subsurface thermal anomalies, SST and surface winds do not show consistent and coherent phase propagation, nor form a cycle. Thus, the continual movement of subsurface thermal anomaly on and off the equator provides a phase-switching mechanism and an interannual memory for the tropical Pacific climate system. Furthermore, such subsurface ocean memory may maintain the self-sustained ENSO occurrence in the coupled tropical Pacific atmosphere–ocean system. In addition, it is such memory that gives the phenomenon predictability and provides a possible physical basis for prediction of interannual variability resulting from the deterministic nature of the subsurface ocean processes.

Acknowledgments. The authors would like to thank our colleagues and staff from the Ocean Climate Laboratory for their help in many aspects. In particular, we would express our special thanks to Tim Boyer, Christine C. Young, Margarita Conkright, John Antonov, and Igor Belkin. We thank Dr. Lewis M. Rothstein for many fruitful discussions and his careful review of early version of the manuscript. The authors wish to thank two anonymous reviewers for their numerous comments and suggestions that helped to improve our original manuscript. Some unpublished calculations by Arlindo Da Silva influenced our work. The authors are indebted to Profs. Qing-Cun Zeng and You-Lin Liang from the Institute of Atmospheric Physics, Chinese Academy of Sciences (Beijing, China) for their help in the work. This research is supported by the NOAA Climate and Global Change Program and the Chinese Ecosystem Research Network Program.

REFERENCES

Battisti, D. S., 1989: On the role of off-equatorial oceanic Rossby waves during ENSO. *J. Phys. Oceanogr.,* **19,** 551–559.

——, and A. Hirst, 1989: Interannual variability in the tropical atmosphere–ocean system: Influence of the basis state, ocean geometry, and nonlinearity. *J. Atmos. Sci.,* **46,** 1687–1712.
Bjerknes, J., 1969: Atmospheric teleconnections from the equatorial Pacific. *Mon. Wea. Rev.,* **97,** 163–172.
Boulanger, J. P., and C. G. Menkes, 1995: Propagation and reflection of long equatorial waves in the Pacific Ocean during the 1992–1993 El Niño. *J. Geophys. Res.,* **100,** 25 041–25 059.
Cane, M. A., and S. E. Zebiak, 1985: A theory for El Niño and the Southern Oscillation. *Science,* **228,** 1085–1087.
——, ——, and S. C. Dolan, 1986: Experimental forecasts of El Niño. *Science,* **321,** 827–832.
Chao, Y., and S. G. H. Philander, 1993: On the structure of the Southern Oscillation. *J. Climate,* **6,** 450–469.
Da Silva, M., C. C. Young, and S. Levitus, 1994a: Atlas of surface marine data 1994. Vol. 1, Algorithms and procedures. NOAA Atlas NESDIS 6. [Available from NODC/NOAA, E/OC5, 1315 East West Highway, Silver Spring, MD 20910.]
——, ——, and ——, 1994b: Atlas of surface marine data 1994. Vol. 2, Anomalies of directly observed quantities, *NOAA Atlas NESDIS 7.* [Available from NODC/NOAA, E/OC5, 1315 East–West Highway, Silver Spring, MD 20910.]
Fu, C.-B., H. F. Diaz, and J. O. Fletcher, 1986: Characteristics of the response of sea surface temperature in the central Pacific associated with warm episodes of the Southern Oscillation. *Mon. Wea. Rev.,* **114,** 1716–1738.
Graham, N. E., and W. B. White, 1988: The El Niño/Southern Oscillation as a natural oscillator of the tropical Pacific Ocean–atmosphere system. *Science,* **240,** 1293–1302.
——, and ——, 1991: Comments on ''On the role of off-equatorial oceanic Rossby waves during ENSO.'' *J. Phys. Oceanogr.,* **21,** 453–460.
Hirst, A. C., 1986: Unstable and damped equatorial modes in simple coupled ocean–atmosphere models. *J. Atmos. Sci.,* **43,** 606–630.
Jin, F.-F., and J. D. Neelin, 1993: Modes of interannual tropical ocean–atmosphere interaction—A unified view. Part I: Numerical results. *J. Atmos. Sci.,* **50,** 3477–3503.
Kessler, W. S., 1990: Observations of long Rossby waves in the northern tropical Pacific. *J. Geophys. Res.,* **95,** 5183–5217.
——, 1991: Can reflected extra-equatorial Rossby waves drive ENSO. *J. Phys. Oceanogr.,* **21,** 444–452.
——, and M. J. McPhaden, 1995: Oceanic equatorial waves and the 1991–93 El Niño. *J. Climate,* **8,** 1757–1774.
Latif, M., A. Sterl, E. Maier-Reimer, and M. M. Junge, 1993: Climate variability in a coupled GCM. Part I: The tropical Pacific. *J. Climate,* **6,** 5–21.
Lau, N.-C., S. G. H. Philander, and M. J. Nath, 1992: Simulation of ENSO-like phenomena with a low resolution coupled GCM of the global ocean and atmosphere. *J. Climate,* **5,** 284–307.
Levitus, S., and T. P. Boyer, 1994: World Ocean atlas. Vol. 4, Temperature, *NOAA Atlas NESDIS 4,* 117 pp. [Available from NODC/NOAA, E/OC5, 1315 East–West Highway, Silver Spring, MD 20910.]
——, J. Antonov, and T. P. Boyer, 1994a: Interannual variability of temperature at 125 m depth in the North Atlantic Ocean. *Science,* **266,** 96–99.
——, T. P. Boyer, and J. Antonov, 1994b: World Ocean atlas. Vol. 5, Interannual variability of upper ocean thermal structure, *NOAA Atlas NESDIS 5,* 176 pp. [Available from NODC/NOAA, E/OC5, 1315 East–West Highway, Silver Spring, MD 20910.]
——, R. Gelfeld, T. Boyer, and D. Johnson, 1994c: Results of the NODC Oceanographic Data Archaeology and Rescue Project. Key to Oceanographic Records Documentation 19, 73 pp. [Available from NODC/NOAA, E/OC5, 1315 East–West Highway, Silver Spring, MD 20910.]
Li, B., and A. J. Clarke, 1994: An examination of some ENSO mechanisms using interannual sea level at the eastern and western equatorial boundaries and the zonally averaged equatorial wind. *J. Phys. Oceanogr.,* **24,** 681–690.
Mantua, N. J., and D. S. Battisti, 1994: Evidence for the delayed oscillator mechanism for ENSO: The ''observed'' oceanic Kelvin mode in the far western Pacific. *J. Phys. Oceanogr.,* **24,** 691–699.
McPhaden, M. J., S. P. Hayes, L. J. Mangum, and J. M. Toole, 1990: Variability in the western equatorial Pacific during the 1986–87 El Niño/Southern Oscillation event. *J. Phys. Oceanogr.,* **20,** 190–208.
Nagai, T., T. Tokioka, M. Endoh, and Y. Kitamura, 1992: El Niño–Southern Oscillation simulated in an MRI atmosphere–ocean coupled general circulation model. *J. Climate,* **5,** 1202–1233.
Neelin, J. D., 1990: A hybrid coupled general circulation model for El Niño studies. *J. Atmos. Sci.,* **47,** 674–693.
——, and Coauthors, 1992: Tropical air–sea interaction in general circulation models. *Climate Dyn.,* **7,** 73–104.
Nigam, S., and H.-S. Shen, 1993: Structure of oceanic and atmospheric low-frequency variability over the tropical Pacific and Indian Oceans. Part I: COADS observations. *J. Climate,* **6,** 657–676.
Philander, S. G. H., N.-C. Lau, R. C. Pacanowski, and M. J. Nath, 1989: Two different simulations of Southern Oscillation and El Niño with coupled ocean–atmosphere general circulation models. *Philos. Trans. Roy. Soc. London, Ser.,* **329,** 167–178.
——, ——, ——, and ——, 1992: Simulation of ENSO with a global atmospheric GCM coupled to a high-resolution, tropical Pacific Ocean GCM. *J. Climate,* **5,** 308–329.
Picaut, J., and T. Delcroix, 1995: Equatorial wave sequence associated with warm pool displacements during the 1986–1989 El Niño–La Niña. *J. Geophys. Res.,* **100,** 18 393–18 408.
Rasmusson, E. M., and T. H. Carpenter, 1982: Variations in tropical sea surface temperature and surface wind stress associated with the Southern Oscillation/El Niño. *Mon. Wea. Rev.,* **110,** 354–384.
——, and J. M. Wallace, 1983: Meteorological aspects of the El Niño/Southern Oscillation. *Science,* **222,** 1195–1202.
Schopf, P. S., and M. J. Suarez, 1988: Vacillations in a coupled ocean–atmosphere model. *J. Atmos. Sci.,* **45,** 549–566.
Springer, S. R., M. J. McPhaden, and A. J. Busalacchi, 1990: Oceanic heat content variability in the tropical Pacific during the 1982–1983 El Niño. *J. Geophys. Res.,* **95,** 22 089–22 101.
Tourre, Y. M., and W. B. White, 1995: ENSO signals in global upper ocean temperature. *J. Phys. Oceanogr.,* **25,** 1317–1332.
Wang, B., 1992: The vertical structure and development of the ENSO anomaly mode during 1979–1989. *J. Atmos. Sci.,* **49,** 698–712.
White, W. B., G. Meyers, J. R. Donguy, and S. E. Pazan, 1985: Short-term climatic variability in the thermal structure of the Pacific Ocean during 1979–1982. *J. Phys. Oceanogr.,* **15,** 917–935.
——, Y. He, and S. E. Pazan, 1989: Off-equatorial westward propagating waves in the tropical Pacific during the 1982–83 and 1986–87 ENSO events. *J. Phys. Oceanogr.,* **19,** 1397–1406.
Woodruff, S. D., R. J. Slutz, R. L. Jenne, and P. M. Steurer, 1987: A Comprehensive Ocean–Atmosphere Data Set. *Bull. Amer. Meteor. Soc.,* **68,** 1239–1250.
Wright, P. B., and J. M. Wallace, 1988: Correlation structure of the El Niño/Southern Oscillation phenomenon. *J. Climate,* **1,** 609–625.
Wyrtki, K., 1975: El Niño—The dynamic response of the equatorial Pacific Ocean to atmospheric forcing. *J. Phys. Oceanogr.,* **5,** 572–584.
——, 1985: Water displacements in the Pacific and the genesis of El Niño cycle. *J. Geophys. Res.,* **90,** 7129–7132.
Zebiak, S. E., 1989: Ocean content variability and El Niño cycles. *J. Phys. Oceanogr.,* **19,** 475–486.
——, and M. A. Cane, 1987: A model ENSO. *Mon. Wea. Rev.,* **115,** 2262–2278.
Zhang, R.-H., and S. Levitus, 1996: Structure and evolution of interannual variability of the tropical Pacific upper ocean temperature. *J. Geophys. Res.,* **101,** 20 501–20 524.
——, Q.-C. Zeng, G.-Q. Zhou, and X.-Z. Liang, 1995: A coupled general circulation model for the tropical Pacific Ocean and global atmosphere. *Adv. Atmos. Sci.,* **12,** 127–142.